THE JOURNAL OF PHYSICAL CHEMISTRY B

Article

pubs.acs.org/JPCB

Submolecular Structure and Orientation of Oligonucleotide Duplexes Tethered to Gold Electrodes Probed by Infrared Reflection Absorption Spectroscopy: Effect of the Electrode Potentials

László Kékedy-Nagy,[†] Elena E. Ferapontova,*[,†] and Izabella Brand*[,‡]

[†]Interdisciplinary Nanoscience Center (iNANO) and Center for DNA Nanotechnology (CDNA), Science and Technology, Aarhus University, Gustav Wieds Vej 14, DK-8000 Aarhus-C, Denmark

[‡]Department of Chemistry, University of Oldenburg, 26111 Oldenburg, Germany

Supporting Information

ABSTRACT: Unique electronic and ligand recognition properties of the DNA double helix provide basis for DNA applications in biomolecular electronic and biosensor devices. However, the relation between the structure of DNA at electrified interfaces and its electronic properties is still not well understood. Here, potential-driven changes in the submolecular structure of DNA double helices composed of either adenine-thymine $(dAdT)_{25}$ or cytosine-guanine $(dGdC)_{20}$ base pairs tethered to the gold electrodes are for the first time analyzed by *in situ* polarization modulation infrared reflection absorption spectroscopy (PM IRRAS) performed under the electrochemical control. It is shown that the conformation of the DNA duplexes tethered to gold electrodes via the C_6 alkanethiol linker strongly depends on the nucleic acid sequence composition. The tilt of purine and pyrimidine rings of the complementary base pairs (dAdT and dGdC) depends on the potential applied to the electrode. By contrast, neither the conformation nor orientation of the ionic in character phosphate−sugar backbone is affected by the electrode potentials. At potentials more positive than the potential of zero charge (pzc), a gradual tilting of the double helix is observed. In this tilted orientation, the planes of the complementary purine and pyrimidine rings lie ideally parallel to each other. These potentials do not affect the integral stability of the DNA double helix at the charged interface. At potentials more negative than the pzc, DNA helices adopt a vertical to the gold surface orientation. Tilt of the purine and pyrimidine rings depends on the composition of the double helix. In monolayers composed of $(dAdT)_{25}$ molecules the rings of the complementary base pairs lie parallel to each other. By contrast, the tilt of purine and pyrimidine rings in $(dGdC)_{20}$ helices depends on the potential applied to the electrode. Such potential-induced mobility of the complementary base pairs can destabilize the helix structure at a submolecular level. These pioneer results on the potential-driven changes in the submolecular structure of double stranded DNA adsorbed on conductive supports contribute to further understanding of the potential-driven sequence-specific electronic properties of surface-tethered oligonucleotides.

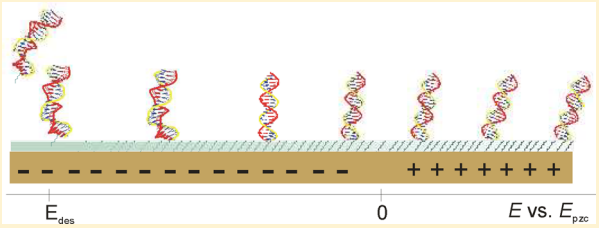

INTRODUCTION

Rapidly expanding fields of DNA-based molecular electronics and biosensors place in focus structural, biorecognition, and electronic properties of DNA molecules localized at the electrified interfaces, which may be different from those observed in solution.[1−3] Both the electrical properties of DNA self-assemblies on electrodes[4] and operation of a large number of electrochemical diagnostic devices for genetic diseases, infections, and personal genetic predispositions[5−7] rely on structural features of the DNA helices tethered to conductive supports.[8] In this context, immobilization of DNA oligomers on electrodes allows for the electrochemical control of the state of hybridization of DNA and its surface concentration. In addition, electrochemical detection enables production of cost-effective miniaturized micro- and nanoarrays for sensitive and specific detection of nucleic acids,[5,7,9,10] DNA-templated electronic nanocircuits,[11,12] and electronically addressable nanomechanical devices based on complex DNA architectures.[13,14]

Immobilization of DNA on conductive surfaces and electrical activation of DNA-based devices may significantly affect both structural and electronic properties of DNA molecules.[6] Current protocols for immobilization of DNA macromolecules on conductive surfaces include either their physical adsorption on mercury, carbon, or metal electrodes[6] or chemisorption via a linker molecule.[15−17] Tethering of alkanethiol-linker modified DNA molecules to a metal surface through the thiol group has become a standard immobilization procedure yielding monolayers of double-stranded DNA (dsDNA) and single-stranded DNA (ssDNA) on gold,[16,18−20] silver,[21] and nickel[22] surfaces.

Received: December 8, 2016
Revised: January 25, 2017

DOI: 10.1021/acs.jpcb.6b12363
J. Phys. Chem. B XXXX, XXX, XXX−XXX

Independently of the electrode material and DNA immobilization procedure used, electrode potentials were shown to have a large impact on the electrochemical stability and surface orientation of adsorbed DNA molecules.[6,18,23−25] First, the electric field was shown to affect the macromolecular orientation of DNA. Atomic force microscopy (AFM)[23,26] and fluorescence spectroscopy[27,28] performed under the electrochemical control demonstrated a potential dependent orientation of dsDNA helices in compact[23] and loosely packed[27] monolayers adsorbed on the gold electrode surface. Initially, it was proposed that at positive potentials DNA helices are tilted toward the Au surface due to the electrostatic attraction between negatively charged phosphate groups of the DNA backbone and positively charged electrode surfaces. By contrast, application of negative potentials leads to the repulsion of the DNA molecules from the electrode surface, being responsible for a vertical orientation of the double helix vs surface normal.[23]

Clearly, negative and positive charges accumulated on the Au electrode surface have an enormous impact on the orientation of dsDNA in monolayer assemblies. Rant et al.[27] showed that the tilting of dsDNA macromolecules on the gold surface is a more complex process involving not only the net charge accumulated on the electrode surface but also electrostatic interactions between the DNA phosphate groups and metal cations from the electrolyte solution. Recent studies show that negative charge of the phosphate groups of the DNA backbone is fully compensated by metal ions adjacent to the helix.[29,30] Therewith, in electrochemical systems, static electric fields acting on the DNA molecules adsorbed on the electrode surface influence charging of the electrical double layer, including the distribution of ions surrounding the dsDNA molecules. The strength of the electric field decays exponentially with the distance from the electrode surface.[31] Analysis of the electric field strength as a function of the distance from the electrode surface and electrolyte concentration indicates clearly that under the most frequently used experimental conditions, at distances larger than 8−10 nm from the electrode surface, the potential drop and thus the electric field acting on DNA molecules are negligible and should not affect the molecular orientation.[27] The average orientation of the DNA molecules adsorbed on metal surfaces is governed by the balance between the electrically induced order (alignment along the electric field) and thermally induced disorder (Brownian motions).[27]

Second and less understood phenomenon is the negative potential-driven denaturation of dsDNA adsorbed on electrodes (at $E < -1.15$ V vs Ag/AgCl). For the first time it was reported independently by Palecek and Nürnberg as far as in 1974.[32,33] After several decades of research neither the mechanism nor structural changes in the DNA biopolymer leading to the potential-driven destabilization of dsDNA helix are known.[6,15,18,19,24] Recent studies of electrochemically induced melting of nucleic acid duplexes composed of negatively charged DNA and synthetic peptide nucleic acid strands, in which backbone is composed of an uncharged pseudopeptide polymer, provide clear evidence that the potential-driven denaturation of DNA molecules adsorbed on the electrode surface is not caused by the electrostatic repulsion.[18] It was suggested that the electrochemically driven dsDNA melting could be connected with structural features of dsDNA and mutual interactions between the base pairs (bp) of the duplex disturbed in the electric fields of high strength.[18] Clearly, the submolecular level analysis of potential-induced changes in the dsDNA structure may shed a light on this phenomenon.

Despite the fact that a large number of advanced *in situ* analyzing techniques, such as AFM,[23] surface plasmon resonance,[34] surface enhanced Raman spectroscopy,[18,24] and fluorescence spectroscopy[27] were used to investigate the surface state and orientation of DNA molecules on electrodes, they were not sensitive enough to detect variations in the dsDNA structure at a submolecular level. Due to weak intensities of often overlapping measured signals, determination of potential-induced fine structural changes in DNA macromolecules is still a challenging experimental task. Infrared spectroscopy (IRS), one of the most important analytical techniques for identification of the molecular structure, can contribute to this task accomplishment. Absorption of the IR light by various molecular groups at different frequencies allows a simultaneous, label-free measurement of absorption modes originating from these groups,[35,36] and reflection based IR spectroscopy allows *in situ* analysis of the composition and structure of organic molecules adsorbed at the liquid|solid interface.[37,38] Moreover, due to the excellent signal-to-noise ratio, polarization modulation infrared reflection absorption spectroscopy (PM IRRAS) is particularly attractive for simultaneous *in situ* studies of changes in the structure, orientation, and hydration of biomolecules adsorbed at solid surfaces.[36,39]

In this article, *in situ* PM IRRAS under electrochemical control was for the first time used to study the electrode-potential induced changes in the structure and orientation of DNA duplexes tethered to polycrystalline gold electrodes via an alkanethiol linker. Here, DNA duplexes composed of either cytosine-guanine $(dGdC)_{20}$ or adenine-thymine $(dAdT)_{25}$ were studied. Density functional theory approach was used to calculate the IR spectra in the nucleic acids base pair absorption spectral region of $(dAdT)_{2-10}$ and $(dGdC)_{2-10}$ helices in D_2O and H_2O solutions.[40,41] The possibility of a theoretical IR spectra evaluation combined with the simple DNA models used in the current work allowed an unambiguous assignment of the detected IR absorption modes to specific nucleic acid bases. All studies in the current work were performed at moderate potentials to avoid electrochemical desorption of the thiolated DNA from the electrode surface. *In situ* PM IRRAS analysis evidenced submolecular structural changes in the DNA duplexes localized at the polarized interface. Aromatic rings of the complementary bp in dsDNA molecules exposed to potentials more negative than the potential of zero charge, E_{pzc}, (at net negative charge on the metal surface) were shown to have different tilt, which depends on the bp composition of dsDNA. Such potential-induced mobility of the nucleic acid bp weakens the intramolecular hydrogen bonds and very likely leads to changes in the distance between the two complementary nucleobases, which in turn can destabilize the overall double helix structure. Exposure of dsDNA molecules to potentials more positive than the E_{pzc} resulted in the entire duplex tilting toward the gold surface, with aromatic rings of the complementary bp adopting an ideally parallel orientation and by this maintaining the native DNA double helix structure.

EXPERIMENTAL SECTION

Materials. All reagents used for buffer solutions preparation and conjugation of methylene blue (MB) to amino-modified DNA were obtained from Sigma-Aldrich (Steinheim, Germany), unless otherwise stated. Distilled water (18.2 MΩ, Type I, ELGA LabWater, Celle, Germany) was used throughout the

DOI: 10.1021/acs.jpcb.6b12363
J. Phys. Chem. B XXXX, XXX, XXX−XXX

electrochemical experiments and deuterium oxide (D_2O, Euroisotop, Saarbrücken, Germany) was used for the PM IRRAS and transmission IRS measurements, respectively. DNA sequences were synthesized by Metabion Int, AG (Martinsried, Germany): 5′-CGG GCG GGC GGG CGG GCG GG-3′ (DNA-1) and 5′-CCC GCC CGC CCG CCC GCC CG-3′ (c-DNA-1); 5′-AAA AAA AAA AAA AAA AAA AAA AAA A-3′ (DNA-2); and 5′-TTT TTT TTT TTT TTT TTT TTT TTT T-3′ (c-DNA-2). Thiol-modified DNA-1 and DNA-2 had a C_6-disulfide ($-(CH2)_6-S-S-(CH_2)_6-OH$) modification at the 3′-end and formed $(dGdC)_{20}$ and $(dAdT)_{25}$ DNA duplexes with their unmodified complementary DNAs (c-DNA). Melting temperatures, T_m, of the DNA duplexes estimated by the DINAMelt web server[42] were 74 °C for the $(dGdC)_{20}$ DNA duplex and 47 °C for the $(dAdT)_{25}$ duplex. Experimentally determined T_m (a Varian Cary 100 Bio spectrophotometer, Analytical Instruments AS, Værløse, Denmark, was used) were consistent with the theoretical ones. For the electrochemical determination of the duplex surface coverage, the c-DNA-1 and c-DNA-2 sequences were modified with a $NH_2-(CH_2)_6$-linker at their 5′-end, to which the succinimide-activated monocarboxy-methylene blue (MB-NHS, emp Biotech GmbH, Berlin, Germany) was conjugated by peptide chemistry.[43,44]

Conjugation of MB to Amine-Modified DNA. Conjugation of MB to the amine-modified DNA oligonucleotide was performed following the protocol described before[45] and slightly modified in this work. In brief, the solution of amine-modified DNA (10 nmol) in deionized water (100 μL) was added to a mixture that contained: MB-NHS (0.25 mg) dissolved in dimethylformamide (DMF ≥ 99%, 50 μL), acetonitrile (MeCN, 99.8%, 50 μL), and trimethylamine (1 μL). The mixture was shaken while incubated for 3.5 h at rt. Precipitation of DNA was performed by adding an aqueous solution of sodium acetate (NaOAc 3 M, 15 μL, pH 5.2), chilled ethanol (EtOH, 495 μL), and glycogen (20 mg mL^{-1}, 1 μL), followed by cooling on dry ice for 15 min. This cooled mixture was centrifuged (Centrifuge 5417 R, Eppendorf, 20000 g) for 1 h at 4 °C and the supernatant was removed immediately after. The pellet was dissolved in the aqueous triethylammonium acetate buffer (TEAA, 200 μL, 0.1 M) and purified by reversed-phase HPLC (10−35% MeCN in 0.1 TEAA over 15 min; 1 mL min^{-1}; 25 °C column temperature). The product-containing fractions were collected and lyophilized.

Preparation of dsDNA Monolayers on the Polycrystalline Au Electrode Surface. Polycrystalline gold disc electrodes (diameter 15 and 4 mm; Alfa Aesar, Kalsruhe, Germany) were thoroughly washed with distilled water and pure ethanol and finally cleaned by flame annealing. Self-assembled DNA monolayers were prepared as follows unless otherwise stated: a drop of a freshly prepared dsDNA sample containing a mixture of 10 μM thiol-modified DNA and 15 μM c-DNA in 10 mM K_2HPO_4/KH_2PO_4 (PBS) containing 0.15 M NaCl and 0.1 M $MgCl_2$, pH 7, was placed on the Au electrode surface. Prior to modification, the dsDNA sample was treated with tris(2-carboxyethyl)phosphine hydrochloride (TCEP) for 1 h, for disulfide bond reduction. For DNA immobilization, the electrode was covered with a lid and left overnight at rt. Next day, the dsDNA-modified electrode was rinsed with 10 mM PBS, pH 7, exposed to 2 mM 6-mercapto-1-hexanol (MC_6OH) solution in 10 mM PBS for 30 min, rinsed again with 10 mM PBS, pH 7, and used in further experiments.

Analysis of the DNA Surface Coverage. The DNA surface concentration (Γ_{DNA}) was determined by integration of the cyclic voltammograms (CV) peaks produced by dsDNAs formed by the MB-labeled cDNA hybridized to the thiolated counterpart, in the formed hybrids the MB redox probe was located at the end adjacent to the electrode surface once the duplex was immobilized. The $\Gamma_{DNA\text{-}MB}$ was obtained according to eq 1:

$$\Gamma_{DNA-MB} = \frac{Q}{nFA} \quad (1)$$

where Q is the charge (C), estimated from the MB cathodic peak area at 0.1 V s^{-1}, n is the number of electrons transfer in the electrochemical process, F is the Faraday number (C mol^{-1}), and A is the electrochemically determined surface area of the gold electrode (cm^2).

Electrochemical Measurements. Electrochemical measurements were performed in a glass three-electrode cell with a polycrystalline Au disc electrode (4 mm diameter) as the working electrode. A gold wire served as the counter electrode and a silver|silver chloride electrode (Ag|AgCl|3MKCl), abbreviated further as (Ag|AgCl), as the reference electrode. All potentials are cited versus this electrode. The reference electrode was separated from the electrolyte solution via a salt bridge. The electrolyte was 0.01 PBS, pH 7. Prior to the experiment, the cell was purged with argon for 30 min. The cleanness of the electrochemical cell was tested by recording CVs of the unmodified Au electrode in PBS. A CHI660A potentiostat (CH Instruments, Austin, USA) with the corresponding software was used to perform electrochemical measurements. CVs were recorded by scanning the potential between 0.45 and −0.80 V with different scan rates. The alternating current voltammograms (ACV) were recorded in positive and negative directions with a scan rate of 5 mV s^{-1} and an AC perturbation of 10 mV amplitude and 20 Hz frequency. The capacitance vs potential dependencies were calculated for the equivalent circuit including a resistor in series with a capacitor, from the in-phase and out-of-phase components of the current signals. The E_{pzc} of the Au electrode in PBS, pH 7.0, was determined here as equal to 0.090 ± 0.005 V.

PM IRRAS. PM IRRA spectra were recorded using a Vertex 70 spectrometer with a polarization modulation set (PMA 50, Bruker, Ettlingen, Germany). All spectra were recorded in a spectroelectrochemical cell at various potentials applied to a polycrystalline gold electrode, which simultaneously served as a mirror for the IR light. A CaF_2 equilateral prism was used as an optical window for the IR radiation. Before assembly of the spectroelectrochemical cell, the prism was washed with water and ethanol and cleaned for 10 min in an ozone chamber (Bioforce Nanosciences, Ames, USA). Monolayers of dsDNA/6-mercapto1-hexanol were prepared on the Au electrode surface. The spectroelectrochemical cell has a built-in platinum counter electrode. The reference electrode was Ag|AgCl in 3 M KCl in either D_2O or H_2O. The cell was filled with 10 mM PBS, pH 7, as electrolyte either in D_2O or H_2O and purged with argon for 1 h to remove oxygen. In each experiment four cathodic (negatively going) and anodic (positively going) potential scans were recorded. Each potential scan was analyzed separately and averaged. Each spectrum shown in this article corresponds to an average of 4000 scans. In the cathodic potential scan the following potentials were applied to the Au electrode 0.1, 0.0, −0.1, −0.2, −0.3, and −0.4 V while in the

DOI: 10.1021/acs.jpcb.6b12363
J. Phys. Chem. B XXXX, XXX, XXX−XXX

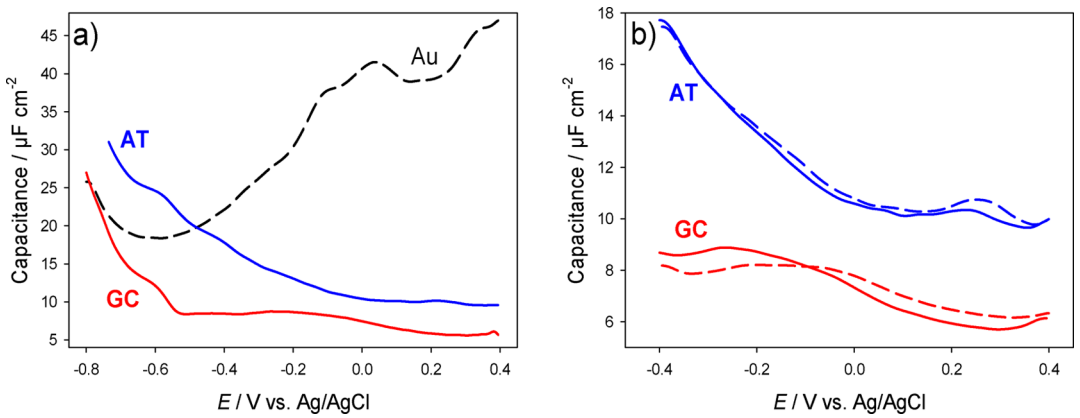

Figure 1. Capacitance vs electrode potential curves recorded in deaerated 10 mM PBS, pH 7, with (a) bare Au (black dashed line), Au electrode modified with $(dAdT)_{25}$ (blue line), and $(dGdC)_{20}$ (red line); (b) $(dAdT)_{25}$ duplexes (blue lines) and $(dGdC)_{20}$ duplexes (red lines), where the solid lines are negative and the dashed lines are positive potential scans.

anodic potential scan −0.3, −0.2, −0.1, 0.0, 0.1, and 0.3 V. For the analysis of the bp C═O and ring stretching modes, the maximum PEM efficiency was set for the half-wave retardation equal to $\tilde{\nu}$ = 1600 cm^{-1}. In this case D_2O was used as a solvent. The thickness of the electrolyte layer between the CaF_2 prism and the Au electrode was 2.0 ± 0.2 μm. The angle of incidence of the IR light φ = 63° vs surface normal. At the half-wave retardation was set to $\tilde{\nu}$ = 1200 cm^{-1} for the analysis of the asymmetric phosphate stretching mode. In this case H_2O was used as a solvent. The angle of incidence was set to φ = 58° and the electrolyte layer thickness was 4.2 ± 0.4 μm. The phosphate ions are present in the electrolyte solution. In order to eliminate from the PM IRRA spectra a contribution from phosphate ions dissolved in the electrolyte solution, the thickness of the electrolyte solution was set to a value at which the average intensities of the electric field vectors of the *p* and *s* polarized light are equal.[46] This procedure allows measuring spectra of species adsorbed directly on the Au surface. The PM IRRA spectra were processed using the OPUS v5.5 software (Bruker, Ettlingen, Germany).

RESULTS AND DISCUSSION

Electrochemical Characterization of dsDNA/6-Mercapto1-Hexanol Monolayers on Au. Monolayers of vertically oriented gold-tethered DNA duplexes representing either $(dAdT)_{25}$ or $(dGdC)_{20}$ dsDNAs were formed on the Au electrode surface according to the previously described procedure.[25,43] In order to remove nonspecifically or weakly adsorbed molecules from the electrode surface, after DNA immobilization the metal surface was treated with 6-mercapto1-hexanol.[20,24,34] Figure 1 shows the variation of the capacitance of the Au electrode modified by dsDNA-6-mercapto1-hexanol monolayers on Au in 10 mM PBS, pH 7.

As can be seen in Figure 1, within the potential range between −0.4 and 0.4 V thiolated DNA duplexes tethered to the Au surface form stable monolayers. Potential cycling in this range does not cause any changes in the capacitance of the electrodes modified with dsDNA monolayers (Figure 1b). Electrodes modified both with $(dAdT)_{25}$ and $(dGdC)_{20}$ reach the capacitance minima at 0 > *E* > 0.4 V, thus at the potentials close to the E_{pzc} of 0.09 V characteristic of the Au electrode in 10 mM PBS, pH 7. The presence of the ω-mercaptoalcohol monolayer adsorbed on the Au electrode surface does not lead to any shift of the potential of zero free charge of the Au electrode in electrolyte solutions with 5 < pH < 8.[47]

Capacitance values characteristic of the two monolayers differ, approaching 10.0−11.5 μF cm^{-2} and 6.2−5.5 μF cm^{-2} for $(dAdT)_{25}$ and $(dGdC)_{20}$ duplexes, respectively. Higher capacitance values observed for the $(dAdT)_{25}$ monolayers may indicate (i) lower surface concentration of the thiolated DNA molecules compared to $(dGdC)_{20}$, (ii) increased disorder (higher number of defects) in the packing of the molecules in the film, and/or (iii) different composition and concentration of ions in the electrical double layer. For the electrode covered by the $(dAdT)_{25}$ monolayer a progressive increase in the capacitance is observed until the monolayer desorption at *E* = −0.595 V, indicating continuous potential driven changes in the adsorption state of the duplexes. By contrast, the capacitance of the Au electrode covered by the $(dGdC)_{20}$ monolayer has a constant value of 8.8 μF cm^{-2} within −0.55 > *E* > −0.20 V. Clearly, in this potential range $(dGdC)_{20}$ duplexes form a more stable monolayer film on the Au surface than the $(dAdT)_{25}$ duplexes (Figure 1a). A peak at *E* = −0.605 V is associated with the reductive desorption of the thiols from the electrode surface. The desorption potential of dsDNA-6-mercapto1-hexanol monolayers is less negative than the desorption potential of *E* ≈ −1.0 V reported for the reductive desorption of *n*-alkanethiols from monocrystalline and polycrystalline gold electrodes in alkaline solutions.[48,49] However, reported above values are in a good agreement with the desorption potentials of thiolated DNA in neutral solutions,[50] emphasizing the important role of pH in the proton-coupled $1e^-$ reaction of the reductive desorption of thiols.[49]

Differences in such interfacial properties of DNA-modified electrodes as the capacitance may arise from the different surface concentration of $(dAdT)_{25}$ and $(dGdC)_{20}$. It can be quantified by direct electrochemical analysis of the redox probe-labeled DNA duplexes. In both monolayers $(dAdT)_{25}$ and $(dGdC)_{20}$ molecules have a very similar dsDNA surface concentration: $\Gamma_{(dGdC)20}$ was 5.6 ± 0.5 pmol cm^{-2} and $\Gamma_{(dAdT)25}$ was 5.3 ± 0.1 pmol cm^{-2}, being in a good agreement with literature.[51,52] Thus, the different interfacial behavior of $(dAdT)_{25}$ and $(dGdC)_{20}$ duplexes should be then correlated rather with the structural properties of the DNA monolayers than with their surface coverage. In order to investigate the impact of the electrode potentials on the submolecular structure of dsDNA molecules, PM IRRA spectra of DNA on

DOI: 10.1021/acs.jpcb.6b12363
J. Phys. Chem. B XXXX, XXX, XXX−XXX

gold were recorded within the potential window of the electrochemical stability of mixed dsDNA/6-mercapto1-hexanol monolayers on the Au surface (Figure 1, $-0.4 < E < 0.3$ V). At these potentials mercaptohexanol molecules form well-organized, stable monolayers on the Au surface (representative PM IRRA spectra originating from the methylene stretching modes of 6-mercapto1-haxanol molecules are shown in the Supporting Information file, part S1, Figure S1). In the $-0.4 < E < 0.3$ V potential range, neither the position nor the intensity of the asymmetric and symmetric methylene stretching modes change. This result is in excellent agreement with the previous *in situ* PM IRRAS studies of *n*-alkanethiol monolayers on the Au electrode surface.[53] It shows clearly that in the studied potential range 6-mercapto1-hexanol molecules adopt well-defined, stable, and potential-independent orientation on the Au electrode surface.

PM IRRA Spectra of $(dAdT)_{25}$ Monolayers on Au. Figure 2a shows a PM IRRA spectrum of randomly distributed

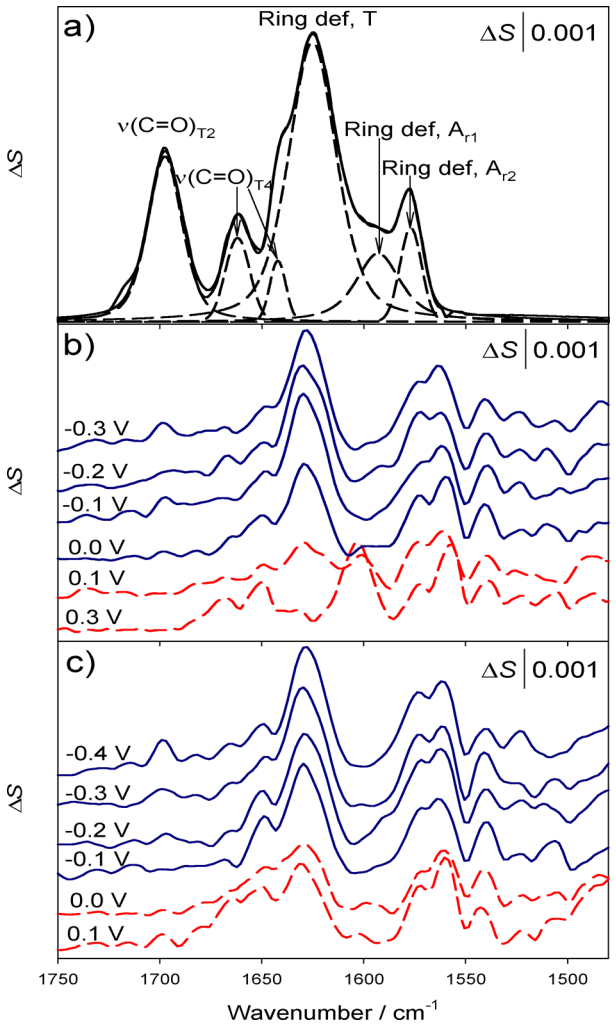

Figure 2. Representative PM IRRA spectra (at 1800–1350 cm^{-1}) of the $(dAdT)_{25}$ duplex (a) calculated for a monolayer thick film of randomly distributed DNA molecules, (d = 8.5 nm and θ = 0.15; see S4 for details), and (b,c) recorded for the $(dAdT)_{25}$/6-mercapto1-hexanol monolayers formed on the Au surface at potentials marked in the figure for (b) positive and (c) negative potential scans. The blue solid lines represent the spectra recorded at $E < E_{pzc}$ and the red dashed lines at $E > E_{pzc}$.

$(dAdT)_{25}$ molecules in a monolayer film, which was calculated from corresponding isotropic optical constants (S2 and Figure S2). Figure 2b,c shows the PM IRRA spectra of $(dAdT)_{25}$ duplexes in monolayers formed on the Au electrode surface. Independent *in situ* PM IRRAS experiments are well reproducible (S3). In this spectral region IR absorption bands originating from the C=O, and in plane ring stretching modes (C=N and C=C) of nucleic acid bases are analyzed. Since the spectra were recorded in D_2O, H atoms of NH_2 groups of dG, dC, and dA are substituted by D and therefore the NH_2 bending modes expected around 1650–1550 cm^{-1} are not visible in the IR spectra of the DNA monolayers.[40,54]

As seen in Figure 2, the PM IRRA spectra of $(dAdT)_{25}$ are composed of a few overlapped absorption bands. A second derivative of the PM IRRA spectrum of $(dAdT)_{25}$ in the film of randomly distributed molecules was calculated in order to find the position and number of individual IR absorption modes contributing to these bands.

The wavenumbers and assignment of the deconvoluted modes are listed in Table 1. As can be seen, the IR absorption modes from dAdT bp in the $(dAdT)_{25}$ monolayers on Au are in a good agreement with the computed IR absorption modes of $(dAdT)_{2-10}$ molecules in D_2O solution.[40]

In the studied $(dAdT)_{25}$ duplex, carbonyl groups are present only in dT, giving rise to two C=O stretching modes. The absorption maximum of the carbonyl stretching modes of the $(C=O)_{T2}$ group not involved in the formation of hydrogen bonds is centered at 1697 cm^{-1}.[40,55] The $\nu(C=O)_{T_4}$ stretching mode is red-shifted to 1662 and 1650 cm^{-1}, characteristic for hydrogen bonded carbonyl groups of dT having different degrees of hydration.[40,56] Three low frequency modes in the PM IRRA spectra of $(dAdT)_{25}$ originate from the in plane ring stretching modes, being in a good agreement with literature.[40]

Concluding, frequencies of the deconvoluted IR absorption modes originating from nucleic acid base pairs do not depend on the potential applied to the Au electrode (Figure 2). However, between independent experiments, a difference of 0–4 cm^{-1} in the position of the maximum of absorption of individual IR absorption modes was observed (S3, Figure S4). Hydration changes at dA and dT bp may lead up to 30 cm^{-1} shift of the corresponding IR absorption modes (Table 1). Thus, the small shift of frequencies of IR absorption modes in this spectral region suggests negligible differences in the hydration of the bp in DNA molecules in different monolayer assemblies.

However, intensities of the IR absorption modes of bp in the monolayer assemblies are significantly attenuated and show large reproducibility (S3). Figure 2 shows clearly that the intensities of the C=O and in-plane ring stretching modes of dA and dT depend strongly on the potential applied to the Au electrode. Large spectral changes are observed at potentials close to the E_{pzc} of the Au electrode in PBS. At $E < E_{pzc}$ the carbonyl stretching modes of dT in the $(dAdT)_{25}$ monolayers are very weak, whereas at positive potentials the intensity of the $\nu(C=O)_{T_4}$ increases. Similarly, the ring stretching mode at 1600 cm^{-1} (A_{r1}) is absent in PM IRRAS spectra at $E < E_{pzc}$ (blue curves in Figure 2) and appears only at $E > E_{pzc}$ (red curves in Figure 2). In the studied potential range thiol-linked $(dAdT)_{25}$ duplexes do not desorb from the Au surface and the surface concentration of the thiolated molecules remains constant. Clearly, observed spectral changes reflect reversible

DOI: 10.1021/acs.jpcb.6b12363
J. Phys. Chem. B XXXX, XXX, XXX–XXX

Table 1. Wavenumbers and Assignment of the IR Absorption Modes Originating from the dAdT Base Pairs of dsDNA

band assignment	wavenumber/cm^{-1}		wavenumber/cm^{-1}	
	$(dAdT)_{25}$ random/this work	$(dAdT)_{25}$ monolayer/Au this work	(dAdT) in D_2O[40]	(dAdT) + $5D_2O$[40,55]
$(C{=}O)_{T2}$	1697.3 ± 0.5s[a]	1697 ± 1vw	1736.9	1699.8
$(C{=}O)_{T4}$	1661.3 ± 0.5m	ca. 1662 ± 2vw	1664.5	1653.2
	1645.4 ± 0.5sh	1650 ± 2w		
ring deformation $_{Tr}$	1624.7 ± 0.5s	1629 ± 2s	1638.1	1631.0
ring deformation $_{Ar1}$	1596.9 ± 0.5m	1602 ± 3vw−m	1600.0	1608.9
ring deformation $_{Ar2}$	1576.7 ± 0.5m	1572 ± 2m	1562.3	1553.8
		1563 ± 2m		

[a]Intensity of the IR absorption band: s−strong, m−medium, w−weak, sh−shoulder, vw−very weak.

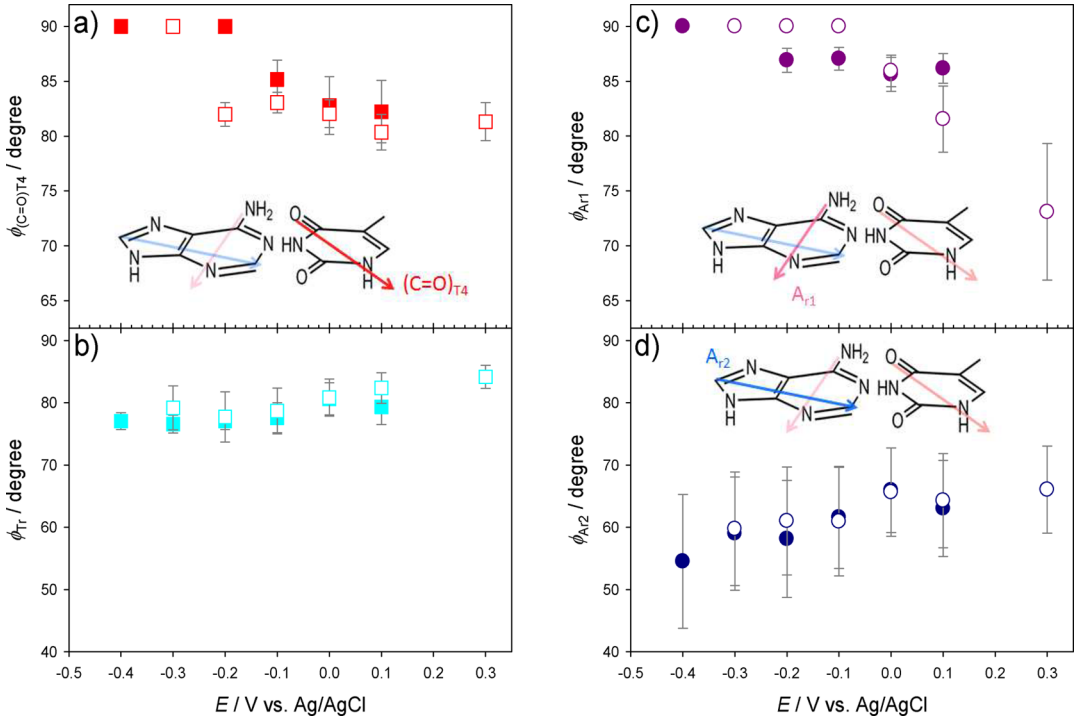

Figure 3. Potential dependence of the tilt angles ϕ vs surface normal obtained for $(dAdT)_{25}$/6-mercapto1-hexanol monolayers on gold for: (a) $\nu(C{=}O)T_4$ stretching modes at 1660−1650 cm^{-1}, (b) ring stretching mode T_r at 1630 cm^{-1}, (c) ring stretching mode A_{r1} at 1603 cm^{-1}, and (d) ring stretching mode A_{r2} at 1580−1565 cm^{-1}. The filled symbols represent the negative and the open symbols represent the positive potential scans, respectively. Insets: structures of the dAdT bp in which directions of the corresponding transition dipole moment vectors are marked by arrows.

potential-driven changes in the orientation of nucleic acid bp in DNA molecules adsorbed on the Au electrode surface.

In an isotropic film, such as the dsDNA monolayer, transition dipole vectors of each IR absorption mode have a strictly defined orientation. According to the surface selection rule of IRRAS, the integral intensity of an IR absorption mode (A) is equal to[57]

$$\int \mathrm{Adv} \propto \Gamma|\vec{\mu}\cdot\vec{E}|^2 = \Gamma\,|\vec{\mu}|^2|\vec{E}|^2\cos^2\phi \qquad (2)$$

It is proportional to the surface concentration of these molecules on the electrode surface (Γ) and the square of the absolute values of the dot product of the transition dipole vector ($\vec{\mu}$) of a given absorption mode and the electric field vector of the incident light ($\vec{E}$). The integral intensity of a given absorption band depends on the angle ϕ between the $\vec{\mu}$ and $\vec{E}$ vectors. On the Au electrode surface, the $\vec{E}$ vector of the p-polarized light is directed normal to the interface. Therefore, changes of the integral intensity of an absorption band reflect the tilt of the $\vec{\mu}$ vector of a given vibrational mode with respect to the surface normal (direction of $\vec{E}$).[58,59] Eq 3 was used to calculate the angles ϕ between the direction of transition dipole vectors of the $(C{=}O)_{T_4}$, ring stretching modes T_r, and A_{r1}, and A_{r2} modes, respectively, and the surface normal:

$$\cos^2\phi = \frac{\int A_{\mathrm{exp}}d\nu}{3\int A_{\mathrm{random}}d\nu} \qquad (3)$$

$A_{\mathrm{exp}}d\nu$ and $A_{\mathrm{random}}d\nu$ represent intensities of the corresponding IR absorption modes of DNA molecules in monolayer assemblies on Au and for the random distribution of the molecules in the film, respectively. For the calculation of the IR spectrum of randomly distributed molecules in the $(dAdT)_{25}$ monolayer on gold, both the thickness of the monolayer and the degree of the electrode coverage by the DNA molecules (the surface coverage, θ) have to be known (S4). In aqueous solutions, a DNA molecule with a surrounding metal ions shell has a diameter of 2.2−3.0 nm.[23,51,60−62] The average area occupied by a dsDNA molecule and its metal ions shell (with a diameter of 2.5 nm (for details see S4)) oriented vertically to

DOI: 10.1021/acs.jpcb.6b12363
J. Phys. Chem. B XXXX, XXX, XXX−XXX

the metal surface is equal to $A(\mathrm{dAdT})_{25}$ = 4.9 nm^2 resulting in the maximum surface concentration $\Gamma_{(\mathrm{dAdT})_{25},\mathrm{max}}$ = 2.04 × 10^{13} molecules cm^{-2}. For the electrochemically determined $\Gamma_{(\mathrm{dAdT})_{25},\ \mathrm{Au}}$ 5.3 ± 0.1 pmol cm^{-2}, the average surface area per $(\mathrm{dAdT})_{25}$ molecule equals 31.5 ± 0.73 nm^2. Taking into account the vertical orientation of the $(\mathrm{dAdT})_{25}$ molecules on Au, it corresponds to the surface coverage θ (fraction of the adsorption sites occupied by DNA) of 0.155 ± 0.004 (S4, Figure S5).

Next, the potential dependence of the tilt angles ϕ between the direction of the transition dipole vector of different modes and the surface normal was evaluated. Taking into account a small difference between PM IRRA spectra recorded in two independent measurements (S3), the error in the determined ϕ is small (0−2°). However, the error due to the estimation of the DNA surface coverage of Au,θ may result in quite large deviations of the determined tilt angles, and therefore the spectra of randomly distributed DNA molecules were calculated for the vertically oriented $(\mathrm{dAdT})_{25}$ molecules and θ = 0.15 ± 0.025 (S4). Error bars shown in Figure 3 include both experimental uncertainties.

The quantitative analysis of the effect of the electrode potential on the orientation of nucleic acid bases in the $(\mathrm{dAdT})_{25}$ monolayer was performed by deconvoluting the PM IRRA spectra shown in Figure 2 (S5, Figure S6). A correlation of the calculated ϕ angles with the orientation of planes of dT and dA rings requires knowledge of the orientation of the transition dipole vectors of carbonyl stretching modes in dT and of plane stretching modes of dA and dT in D_2O solution. Theoretical IR spectra of dAdT DNA-fragments in D_2O solution in the 1800−1400 cm^{-1} spectral region, and the orientation of the corresponding transition dipole vectors were calculated by Lee and Cho.[40,54] In further analysis, we used directions of the transition dipole vectors in dAdT in the D_2O solution reported in these works. The structure of the dAdT base pair and the directions of the transition dipole moments of the C═O and ring stretching modes are shown in Figure 3.

As shown in Figure 3a the transition dipole vector of the $\nu(\mathrm{C{=}O})_{\mathrm{T}_4}$ lies in the plane of the pyrimidine ring of dT and is oriented parallel to the C═O bond.[40] This mode reflects the tilt of the aromatic ring of dT along the axis that is a prolongation of the carbonyl bond vs surface normal. The calculated tilt angle $\phi_{(\mathrm{C{=}O})\mathrm{T}_4}$ depends on the potential applied to the Au electrode. At E < −0.2 V, the $\phi_{(\mathrm{C{=}O})\mathrm{T}_4}$ is equal to 90°, indicating that the plane of the dT pyrimidine ring is oriented parallel to the metal surface. A positive potential shift leads to a decrease in the $\phi_{(\mathrm{C{=}O})\mathrm{T}_4}$ to ca. 80°. For the complementary base, dA, the transition dipole vector of the ring stretching mode, $\mathrm{A_{r1}}$ at 1603 cm^{-1}, is oriented along the C-ND_2 bond and reflects the tilt of the plane of the purine ring vs surface normal (Figure 3c).[40] This mode is visible in the PM IRRA spectra of the $(\mathrm{dAdT})_{25}$ monolayer only at $E \geq$ 0.1 V (Figure 2). The absence of the $\mathrm{A_{r1}}$ mode at E < 0.0 V indicates that the $\phi_{\mathrm{A_{r1}}}$ is equal to 90° (Figure 3c) and the plane of the purine ring adopts orientation that is parallel to the Au surface. A positive potential shift leads to a decrease in the ϕ_{Ar1} to ca. 75°. By contrast, the ring stretching modes in dT ($\mathrm{T_r}$ at 1629 cm^{-1}) and dA ($\mathrm{A_{r2}}$ at 1570 cm^{-1}) are the most intense at negative potentials, while their intensities decrease at positive potentials. The transition dipole vector of the $\mathrm{A_{r2}}$ mode is almost perpendicular to the line representing a prolongation of the C-ND_2 bond and reflects rotation of the purine ring along this axis as shown in Figure 3d.[40] The angle $\phi_{\mathrm{A_{r2}}}$ is close to 53° at E = −0.4 V and increases gradually to ca. 65° at E = 0.4 V (Figure 3d). The angle $\phi_{\mathrm{T_r}}$ increases from ca. 75° at negative potentials to 85° at positive potentials. These results indicate that electrode potentials influence not only the tilt of the plane of the aromatic rings of dT and dA, but also impose their twist.

In the 1300−1130 cm^{-1} spectral region, the PM IRRA spectra correspond to the asymmetric phosphate stretching mode $\nu_{\mathrm{as}}(\mathrm{PO_2^-})$ and the C−O stretching mode of the deoxyribose-phosphate backbone of $(\mathrm{dAdT})_{25}$ molecules (Figure 4). Phosphate groups of the $(\mathrm{dAdT})_{25}$ duplex give

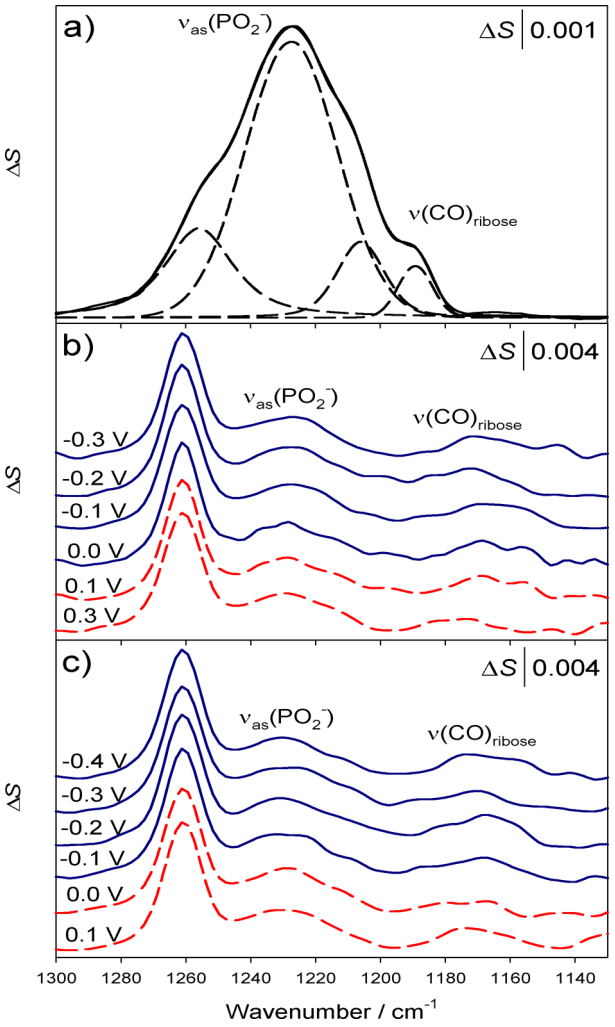

Figure 4. Representative PM IRRA spectra of the $(\mathrm{dAdT})_{25}$ duplex (in 1300−1130 cm^{-1} region) (a) calculated for a monolayer thick film of randomly distributed DNA molecules (d = 8.5 nm and θ = 0.15, S4), and (b,c) recorded for the $(\mathrm{dAdT})_{25}$/6-mercapto1-hexanol monolayer on the Au electrode at potentials marked in the figure for (b) positive and (c) negative potential scans. The blue solid lines represent the spectra recorded at $E < E_{\mathrm{pzc}}$ and the red dashed lines at $E > E_{\mathrm{pzc}}$.

rise to a strong and broad absorption mode between 1265−1210 cm^{-1}. This mode is composed of three overlapped absorption modes, reflecting the crystal structure of the DNA duplex as well as differences in the hydration of phosphate groups of dsDNA.[54,63,64] In the PM IRRA spectrum of randomly distributed $(\mathrm{dAdT})_{25}$ molecules, the deconvoluted

DOI: 10.1021/acs.jpcb.6b12363
J. Phys. Chem. B XXXX, XXX, XXX−XXX

$\nu_{as}(PO_2^-)$ mode has the following maxima of absorption: 1256, 1227, and 1206 cm^{-1}, corresponding to dehydrated (bound to cations), hydrated, and hydrogen bonded phosphate groups, respectively.[63] The IR absorption mode centered at 1227 cm^{-1} gives the strongest contribution to the $\nu_{as}(PO_2^-)$ mode indicating that in aqueous solutions the largest fraction of phosphate groups of $(dAdT)_{25}$ molecules is well-hydrated and exists in the B-form.[65]

In this spectral region, $(dAdT)_{25}$ duplexes attached to the Au surface exhibit significantly different spectral signals compared to the calculated spectrum (Figure 4). The high frequency mode at 1261 cm^{-1} becomes the strongest component of the entire $\nu_{as}(PO_2^-)$ band. It overlaps with two weak absorption modes centered at 1229 and 1209 cm^{-1}. At the low frequency side, the $\nu_{as}(PO_2^-)$ mode overlaps with the ν(C−O) of the deoxyribose-phosphate backbone of the double helix. The frequency of the ν(C−O) of the 2′-position of the deoxyribose residue depends on the crystal structure of DNA.[66] The C−O stretching vibrations of the deoxyribose-phosphate backbone are expected at 1187 cm^{-1} for the A-DNA crystal structure and around 1200 cm^{-1} and 1165−1150 cm^{-1} for the B-DNA form.[64,66] In aqueous solutions of $(dAdT)_{25}$ the ν(C−O) mode is centered at 1192 cm^{-1} while the $\nu_{as}(PO_2^-)$ at 1226 cm^{-1}, indicating that the double helix exists in the B-conformation.[64−66] Adsorption of the $(dAdT)_{25}$ duplex on the Au surface leads to a red-shift of the ν(C−O) mode, to 1170−1155 cm^{-1}. Simultaneously, a large fraction of DNA's phosphate groups becomes dehydrated. However, the $\nu_{as}(PO_2^-)$ mode due to the hydrated phosphate groups is centered at 1228 cm^{-1}, characteristic of the B-DNA structure.[65]

Despite spectral changes, frequencies of the $\nu_{as}(PO_2^-)$ and ν(C−O) modes indicate that $(dAdT)_{25}$ molecules adsorbed on the Au surface adopt one of the polymorphous B-structures, which is indeed the most stable conformation of DNA duplexes containing more than 70% dAdT bp.[67] As shown in Figure 4, in the 1300−1130 cm^{-1} region the potential of the Au electrode has almost no impact on the PM IRRA spectra of $(dAdT)_{25}$ molecules.

As reported earlier, the transition dipole vector of the $\nu_{as}(PO_2^-)$ mode lies along the O···O line of this group.[54,65] The potential dependence of the tilt angle of the O···O line in phosphate groups in $(dAdT)_{25}$ monolayers is shown in Figure 5. The O···O line in $(dAdT)_{25}$ molecules in the monolayer assembly has a quite rigid orientation. The tilt angle varies between 53° and 58°. This result may indicate that either the phosphate groups of the DNA helix adopt a random orientation[36] or they are uniformly oriented and produce a tilt of ca. 55°.

PM IRRA Spectra of $(dGdC)_{20}$ Monolayers on Au Electrodes. Figure 6 shows PM IRRA spectra of $(dGdC)_{20}$ molecules (at 1800−1350 cm^{-1}) randomly distributed in a monolayer thick film calculated from isotropic optical constants (Figure S3) and in DNA monolayers adsorbed on the Au electrode surface. In the PM IRRA spectrum of randomly distributed molecules two high frequency modes at 1685 and 1654 cm^{-1} originate from the ν(C═O) stretching modes in dG and dC, respectively (Table 2).

In the $(dGdC)_{20}$ monolayer tethered to the Au surface, the corresponding modes appear at 1682, 1664, and 1648 cm^{-1}, reflecting differences in the hydration of carbonyl groups at the dGdC bp.[40,56] The presence of the ν(C═O) at 1682 cm^{-1} indicates that a large fraction of carbonyl groups of dG involved in the formation of hydrogen bonds is poorly hydrated (Table 2). Two low frequency modes at 1664 and 1648 cm^{-1} are due to the ν(C═O) at dC, indicating that in the monolayer assembly carbonyl groups of pyrimidine rings have different degrees of hydration. Two low frequency modes seen in Figure 6 correspond to the ring stretching modes in dC and dG. Deconvolution of PM IRRA spectra (Figure S7) allows for the quantitative analysis of the orientation of dGdC base pair in monolayers on the Au electrode surface.

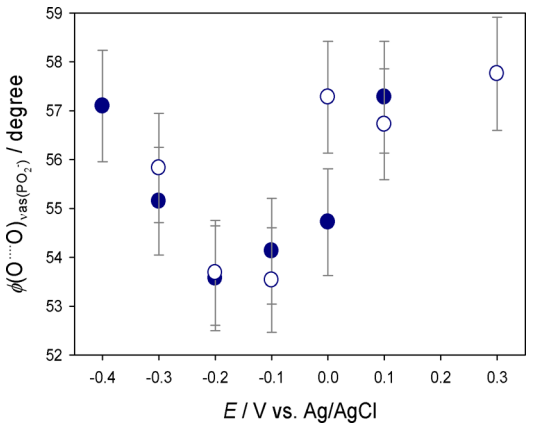

Figure 5. Potential dependence of the tilt angles ϕ(O···O) line in the phosphate group vs surface normal in $(dAdT)_{25}$/6-mercapto1-hexanol monolayers on the Au electrode. The filled symbols represent the negative and the open symbols represent the positive potential scans, respectively.

At $E > E_{pzc}$ the tilt angles of the C═O stretching modes in dC and dG are the same and equal 72° ± 4° (Figure 7a). The tilt angles of the ring stretching modes in dC and dG are equal to 80° and in G to 73°, respectively (Figure 7b).

A negative potential shift to $E < E_{pzc}$ leads to an increase in the intensities of the absorption modes in dC and simultaneously a decrease in the intensities of the corresponding modes in dG (Figure 6). Directions of the transition dipole moments of the ν(C═O) modes in dG and dC are shown in Figure 7a. They are oriented along the C═O bond and reflect the tilt of the aromatic rings with respect to the surface normal. The tilt angle of the C═O in dC increases to 78° at $E = -0.4$ V. At the same the time the tilt angle of the ν(C═O) in dG decreases to 65°. Transition dipole vectors of the ring stretching modes in dC and dG have a similar orientation to the directions of the ν(C═O) mode in corresponding bases as illustrated in Figure 7b. Indeed, Figure 7b shows that the calculated tilt angles are very similar to those shown in Figure 7a. It shows that the band deconvolution and data analysis procedures are consistent.

Finally, the theoretical and experimental PM IRRA spectra of $(dGdC)_{20}$ molecules randomly distributed in a monolayer and in anisotropic monolayers adsorbed on the Au surface were analyzed in the 1300−1110 cm^{-1} spectral region (Figure 8).

In the PM IRRA spectrum corresponding to a random distribution of $(dGdC)_{20}$ molecules the maximum of absorption of the broad $\nu_{as}(PO_2^-)$ mode appears at 1223 cm^{-1}. Deconvolution of this mode results in two IR absorption modes centered at 1228 and 1216 cm^{-1}. The weak IR absorption mode at 1180 cm^{-1} arises from the C−O stretching mode connecting deoxyribose-phosphate groups.[66] Positions of the $\nu_{as}(PO_2^-)$ and ν(C−O) modes indicate that in aqueous solutions the $(dGdC)_{20}$ duplex exists in the B-form.[65,68] In monolayer assemblies of $(dGdC)_{20}$ a new band on the high

DOI: 10.1021/acs.jpcb.6b12363
J. Phys. Chem. B XXXX, XXX, XXX−XXX

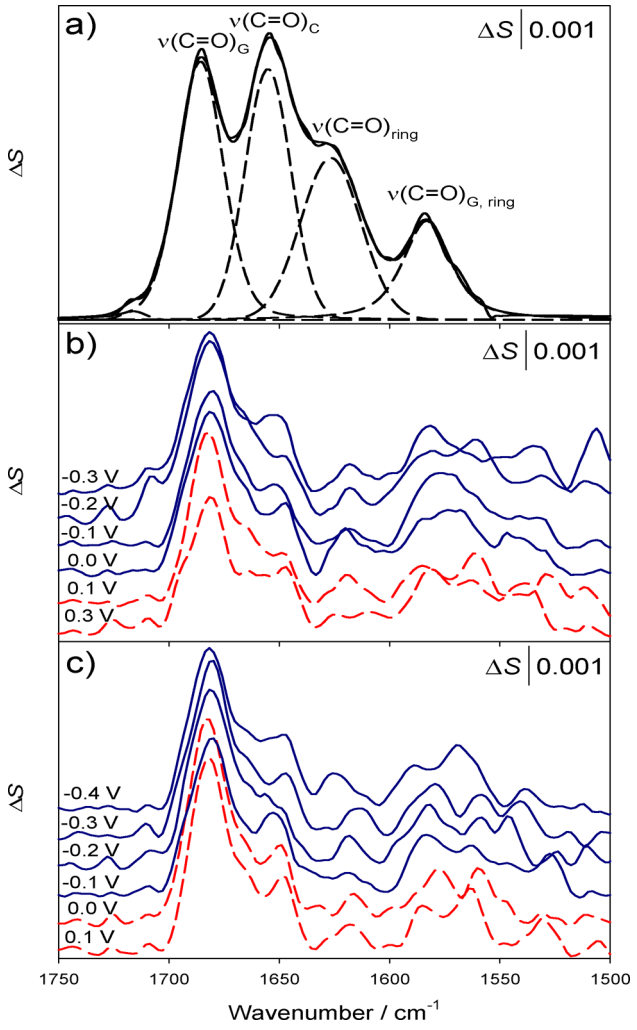

Figure 6. Representative PM IRRA spectra (in 1800−1350 cm^{-1} spectral region) of the $(dGdC)_{20}$ duplex (a) calculated for a monolayer thick film of randomly distributed molecules (d = 6.8 nm and θ = 0.15, see S4 for more details) (b,c) recorded for the $(dGdC)_{20}$/6-mercapto1-hexanol monolayers on the Au surface at potentials marked in the figure for (b) positive and (c) negative potential scans. The blue solid lines represent the spectra recorded at $E < E_{pzc}$ and the red dashed lines at $E > E_{pzc}$.

frequency side is clearly seen in the $\nu_{as}(PO_2^-)$ absorption band. Deconvolution of the $\nu_{as}(PO_2^-)$ gives three modes centered around 1243, 1228, and 1210 cm^{-1}. The IR absorption mode at 1243 cm^{-1} is ascribed to the DNA helices existing in the A-form[65] and indicates that a fraction of $(dGdC)_{20}$ molecules in monolayers chemisorbed on Au exists in the A-form. Independently of the crystal structure of dsDNA, dehydration of the phosphate group leads to a blue-shift of the $\nu_{as}(PO_2^-)$.[63] In a DNA helix existing in the A-form, the axial rise per residue is equal to 0.255 nm compared to 0.340 nm in the B-form.[64] A decrease in the separation between bp provides less space for water molecules to hydrate the phosphate moiety, which is reflected in the blue-shift of the $\nu_{as}(PO_2^-)$ in $(dGdC)_{20}$ duplexes tethered to the Au electrode surface.

The $\nu_{as}(PO_2^-)$ mode centered at 1226 cm^{-1} is characteristic of the dsDNA existing in the B-form and corresponds to the frequency expected for well-hydrated phosphate groups.[65] The presence of the third $\nu_{as}(PO_2^-)$ absorption mode around 1210 cm^{-1} indicates that a fraction of phosphate groups is able to form strong hydrogen bonds with water.[63] At $E < -0.2$ V the ν(CO) mode appears at 1180−1175 cm^{-1}. In parallel, an increase in the absorption around 1200 cm^{-1} is observed. At $E \geq 0.0$ V the maximum of absorption of the ν(C−O) mode is red-shifted to 1175−1160 cm^{-1}. The number and frequencies of the $\nu_{as}(PO_2^-)$ and ν(C−O) modes indicate that $(dGdC)_{20}$ molecules adsorbed on gold exist in both A- and B-conformations.[65,66]

Integral intensities of the $\nu_{as}(PO_2^-)$ were used to calculate the average tilt of the O···O line at the phosphate backbone in $(dGdC)_{20}$ monolayers formed on the Au surface (Figure 9). It can be seen that in $(dGdC)_{20}$ duplexes the orientation of the O···O line depends on the potential applied to the Au electrode. At $E > 0.0$ V the O···O line in phosphate groups makes an average angle of 40° ± 6°. At $E < E_{pzc}$, the tilt of the O···O line increases to ca. 50°. A hysteresis in the changes of the tilt angle of the O···O line between the negative and positive potential scans suggests that the potential-induced reorientation of the phosphate groups is a slow process.

Potential-Driven Changes in the Submolecular Structure of Au-Tethered DNA Duplexes. PM IRRA spectra of $(dAdT)_{25}$ and $(dGdC)_{20}$ duplexes exhibit a remarkably different features at different electrode potentials, indicating that the DNA sequence composition and the surface charge of the Au electrode have a large impact on the structure, orientation, and presumably stability of the DNA molecules immobilized on the metal electrode. As follows from our data, in $(dAdT)_{25}$ monolayers the double helix exists in the B-form, at any potential applied to the Au electrode. By contrast A- and B-forms coexist in $(dGdC)_{20}$ monolayers on the Au electrode surface. Knowledge of the conformation of $(dAdT)_{25}$ and $(dGdC)_{20}$ duplexes tethered to gold and the quantitative analysis of the PM IRRA spectra presented above allow us to specifically discuss the electrode potential-driven changes in the orientation of bp and phosphate groups in the surface attached, vertically oriented DNA molecules.

$(dAdT)_{25}$ Case. At $E > E_{pzc}$ (at positive net charge accumulated on the Au electrode surface) the planes of the aromatic rings in dA and dT give the tilt angle of 70° − 75° vs

Table 2. Wavenumbers and Assignment of the IR Absorption Modes Originating from dGdC Base Pairs of dsDNA

	wavenumber/cm^{-1}		wavenumber/cm^{-1}	
band assignment	DNA random/this work	DNA monolayer/Au this work	DNA in D_2O[40]	DNA + 5D_2O[40,55]
$(C{=}O)_G$	1685.2s	1682.2 ± 0.5s	1687.6	1661.4
$(C{=}O)_C$	1654.0s	1663.6 ± 1.2w	1666.4	1638.7
		1648.5 ± 1.2w		
ring deformation $_C$	1622.5m	1621.2 ± 1.6vw	1634.2	1623.8
ring deformation $_G$	1582.3m	1583.5 ± 1.5w	1561.6	1573.5
		1565.6 ± 1.5w		

DOI: 10.1021/acs.jpcb.6b12363
J. Phys. Chem. B XXXX, XXX, XXX−XXX

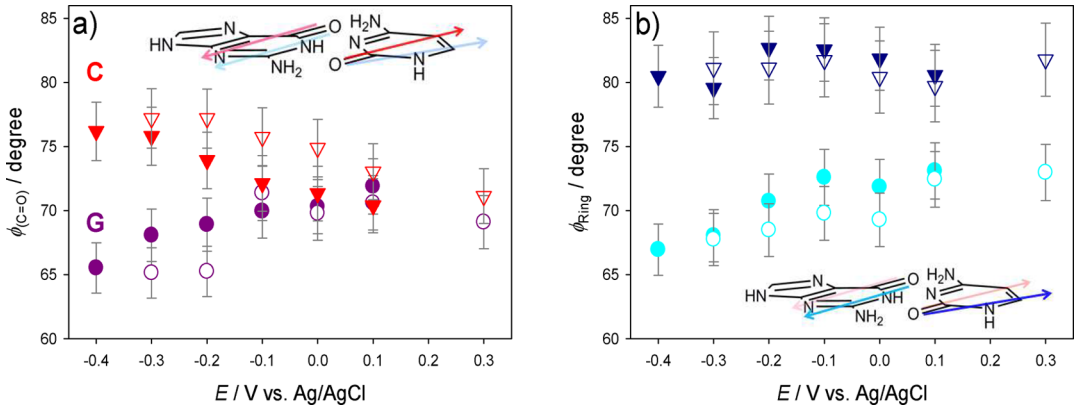

Figure 7. Potential dependencies of the tilt angles ϕ vs surface normal obtained for $(dGdC)_{20}$/6-mercapto1-hexanol monolayers on the Au electrode for (a) ν(C═O) stretching modes in dC at 1660−1645 cm^{-1} (red triangles), and in dG at 1681 cm^{-1} (pink circles); (b) ring stretching modes in dC at 1622 cm^{-1} (blue triangles), and in dG at 1580−1540 cm^{-1} (cyan circles). The filled symbols represent the negative and the open symbols represent the positive potential scans, respectively. Insets: structures of the dGdC bp in which directions of the corresponding transition dipole moment vectors are marked by arrows.

surface normal (Figure 3). In the B-DNA conformation the planes of the complementary bp lie parallel to each other and are tilted by 84° with respect to the helix axis.[64] This result indicates that the helix axis in the $(dAdT)_{25}$ duplex is titled by 10−15° from the surface normal. Indeed, a tilt of the DNA double helices toward the metal surface was earlier reported for the DNA monolayer assemblies at a positive net charge accumulated on the electrode surface.[23,27] In the B-DNA form the O···O line of the phosphate group is tilted by 56° vs helix axis.[65] At $E > E_{pzc}$ the determined tilt of the O···O line is close to 60° vs surface normal. Taking into account that at $E > E_{pzc}$ the helix has a tilt of ca. 10−15° vs surface normal, the expected tilt of the O···O line should be close to 65−70° vs surface normal, being in agreement with the native DNA structure.[67,69]

At the molecular bp level, the integrity of the DNA double helix depends not only on the tilt of the planes of the two aromatic rings vs helix axis but also on the relative tilt of the purine and pyrimidine rings of the complementary bases.[70] When the planes of two complementary bases are oriented ideally parallel, the difference between two modes with the same orientation of the transition dipole vectors (Figure 3a,c), $(\phi_{T_{C=O4}} - \phi_{A_{r1}})$, should be equal to zero. Results of this analysis are shown in Figure 10a. The difference in the tilt angle of the planes of dT and dA rings approaches zero, indicating that the planes of the aromatic rings of the complementary bases are oriented parallel to each other, despite ca. 15° inclination of the double helix toward the metal surface.

At $E < E_{pzc}$ (at negative net charge accumulated on the Au electrode surface) the planes of the aromatic rings of dT and dA adopt a tilt angle of 90° vs surface normal (Figure 3). The O···O line makes an angle of 55°, as expected for the B-form DNA with vertically oriented helices.[65] The orientation of the O···O line in the phosphate group does not change with the potential applied to the Au electrode. Concluding, presented above results indicate that the $(dAdT)_{25}$ molecules adopt a vertical to the metal surface orientation, in agreement with literature.[23,27] As seen in Figure 10a, the planes of the dA and dT rings are parallel to each other, maintaining the native structure of the $(dAdT)_{25}$ double helix.

$(dGdC)_{20}$ case. Since both the A-DNA and B-DNA conformations exist in $(dGdC)_{20}$ monolayers on Au, the exact determination of the orientation of the dsDNA helices is difficult. In the B-form the planes of the dGdC bp are oriented almost perpendicular to the helix axis.[64] In the A-form the planes of the parallel-oriented bp make a tilt of ca. 70° with respect to the helix axis. At $E > E_{pzc}$ the tilt of the planes of the dC and dG rings is similar and close to 70° vs surface normal. This angle is comparable to that expected for the pure A-DNA form and is lower than 90° expected for the pure B-form. This result indicates that the helix axis of $(dGdC)_{20}$ molecules adsorbed on the Au surface is tilted by several degrees from the surface normal. Figure 11a shows the difference between the $\phi_{C=O,G}$ and $\phi_{C=O,C}$ angles as a function of the electrode potential, corresponding to the difference in the tilt of two aromatic rings of the complementary bases in the $(dGdC)_{20}$ duplexes (Figure 7). At $E > E_{pzc}$ this difference is close to zero indicating that the planes of the dC and dG rings are orientated parallel to each other.

At $E < E_{pzc}$ the tilt angle of the C═O bond of dC, reflecting the tilt of the ring along the axis prolonging the carbonyl bond, increases to ca. 80° (Figure 7a). Simultaneously, the tilt angle of the C═O bond of dG, corresponding to the tilt of the aromatic ring along the axis prolonging the carbonyl bond, decreases to ca. 65° vs surface normal (Figure 7a). Clearly, negative electrode potentials lead to a nonparallel orientation of the planes in dG and dC rings. The difference in the tilt of the planes of the aromatic rings in dC and dG bp increases with the negative potential shift as can be seen in Figure 11a. Figure 11b shows the structures of the $(dGdC)_{20}$ duplexes in the A- and B-form, calculated under assumption that the difference in the tilt of planes of the dC and dG bases equals either 0° (E = 0.3 V) or 18° (E = −0.4 V), respectively. Different tilt angles of the planes of purine and pyrimidine rings can lead to destabilization of both, the A- and B-DNA double helix structure at negative potentials. That contrasts to the results obtained for the $(dAdT)_{25}$ duplexes on gold.

CONCLUSIONS

In this work the first experimental evidence on the effect of the electrode potentials (surface charge) on the supramolecular and submolecular structures of dsDNA molecules tethered to the Au electrode surface is reported. Obtained *in situ* PM IRRA data show that electrode potential induced structural changes in the DNA molecule depend primarily on the sequence

DOI: 10.1021/acs.jpcb.6b12363
J. Phys. Chem. B XXXX, XXX, XXX−XXX

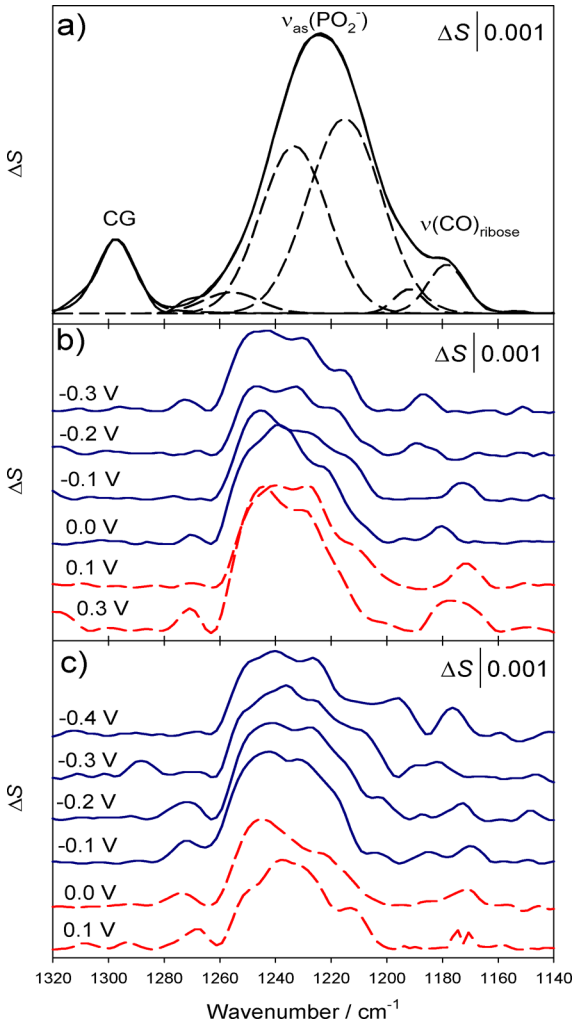

Figure 8. Representative PM IRRA spectra of the $(dGdC)_{20}$ duplex (in 1320−1140 cm^{-1} spectral region) (a) calculated for a monolayer thick film of randomly distributed molecules (d = 6.46 nm and θ = 0.15, see S4 for more details) and (b,c) for the $(dGdC)_{20}$/6-mercapto1-hexanol monolayers formed on the Au surface at potentials marked in the figure for (b) positive and (c) negative potential scans. The blue solid lines represent the spectra recorded at $E < E_{pzc}$ and the red dashed lines at $E > E_{pzc}$.

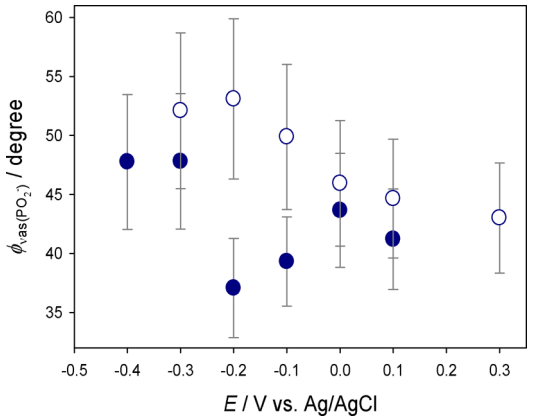

Figure 9. Potential dependence of the tilt angles ϕ(O···O) line in the phosphate group in $(dGdC)_{25}$/6-mercapto1-hexanol monolayers on the Au electrode. The filled symbols represent the negative and the open symbols represent the positive potential scans, respectively.

composition of DNA, and to a lesser extent on the sugar−phosphate backbone−electrode interactions.

First, the conformational state of the DNA duplexes immobilized on electrodes depends strongly on the DNA sequence composition. At a supramolecular level, the potential applied to the DNA-modified electrode influences the surface alignment of the immobilized DNA double helices and hydration of the ionic in character phosphate−sugar backbone. Compared to the DNA state in aqueous solutions, the phosphate groups of $(dAdT)_{25}$ and $(dGdC)_{20}$ in DNA monolayers on gold appear to be poorly hydrated. The presence of a large number of dehydrated phosphate groups in the dominating at electrode stable B-form of the $(dAdT)_{25}$ duplex[67] may be explained by the enhanced binding of Na^+ ions from the electrolyte solution to the DNA localized at the polarized interface. Both charge−charge interactions and hydration of the phosphate groups at DNA duplexes (composed of 20−25 bps) stabilize the entire supramolecular assembly structure. The macromolecular alignment of DNA helices in monolayer assemblies on gold strongly depends on the net surface charge of the metal electrode.[23,27] In diluted, 24−48 bp long dsDNA monolayers on gold ($\Gamma_{DNA} \sim 5 \times 10^{11}$ molecules cm^{-2}), DNA molecules possess a large rotational freedom, and the tilt angle of the double helix at positive potentials can be large (70° vs surface normal).[27] In more compact DNA monolayers (surface concentration >1 × 10^{12} molecules cm^{-2}) the rotational freedom of DNA molecules is significantly restricted and a large inclination of the double helix toward the Au surface is not possible. AFM studies of compactly packed DNA monolayers on Au reveal a 45° tilt of the double helix vs surface normal, at E = 0.45 V vs Ag wire pseudoreference electrode.[23] Surface concentrations of $(dAdT)_{25}$ and $(dGdC)_{20}$ duplexes on Au electrodes studied here are (3.19 ± 0.06) × 10^{12} and (3.37 ± 0.30) × 10^{12} molecules cm^{-2}, respectively. At these surface densities a large tilt of the double helix is excluded. In addition, the most positive potential examined in our work is only 0.2 V higher than the E_{pzc}, and even such a small deviation from the E_{pzc} appeared to be sufficient to induce the potential-driven tilting of the double helix.

Second, our results show that at a submolecular level, an electrode potential shift can lead to changes in the tilt of the purine and pyrimidine rings of the complementary bases. At $E > E_{pzc}$ a parallel to each other orientation of the aromatic rings of bp is preserved in the DNA duplex, both for $(dAdT)_{25}$ and $(dGdC)_{20}$ molecules. By contrast, at $E < E_{pzc}$, in $(dGdC)_{20}$ duplexes the mobility of the nucleic acid base pairs increases, which can contribute to a destabilization of hydrogen bonds between complementary bases affecting the overall DNA structure. A breakdown of the double helix structure occurs at $E < -1.1$ V.[18] This potential range is not explored in the current work, due to electrochemical instability of thiol-linked dsDNA molecules in studied monolayer assemblies.

Described above results clearly demonstrate the specific effects of the electrode potentials (surface charges) on the submolecular structure of DNA double helices of different composition. It may have a particular importance for a further development of functional DNA-based devices. Though it is well-understood, that more experimental evidence should be collected, also with DNA duplexes of more complex sequence compositions, length, and electrode environmental conditions (electrolyte ionic strength, ionic composition, pH, T, etc.). However, even in the present state the acquired knowledge

DOI: 10.1021/acs.jpcb.6b12363
J. Phys. Chem. B XXXX, XXX, XXX−XXX

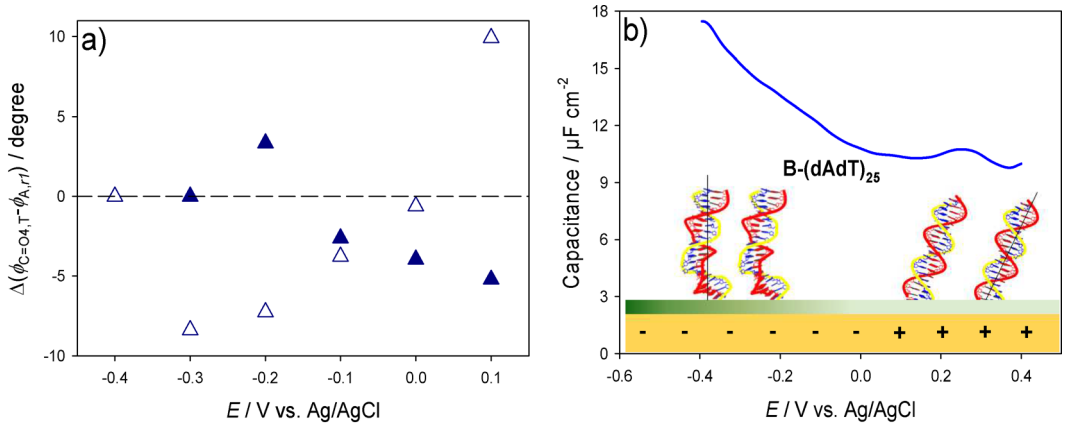

Figure 10. (a) Potential dependence of the difference between the orientation of the transition dipole vectors ($\phi_{T_{C=O4}} - \phi_{A_{r1}}$) calculated from the data on the tilt angles of the carbonyl and in-plane ring stretching modes in $(dAdT)_{25}$ monolayers on the Au surface. The filled symbols are negative and the open symbols are positive potential scans, respectively. (b) Representative capacitance−potential dependence of the $(dAdT)_{25}$-modified Au electrode and a schematic illustration of the orientation of the $(dAdT)_{25}$ duplexes on Au at E = 0.3 V and E = −0.4 V. dA is marked in red and dT is marked in blue. The DNA structures were calculated based on the results obtained in this work using the 3dna software package.[70]

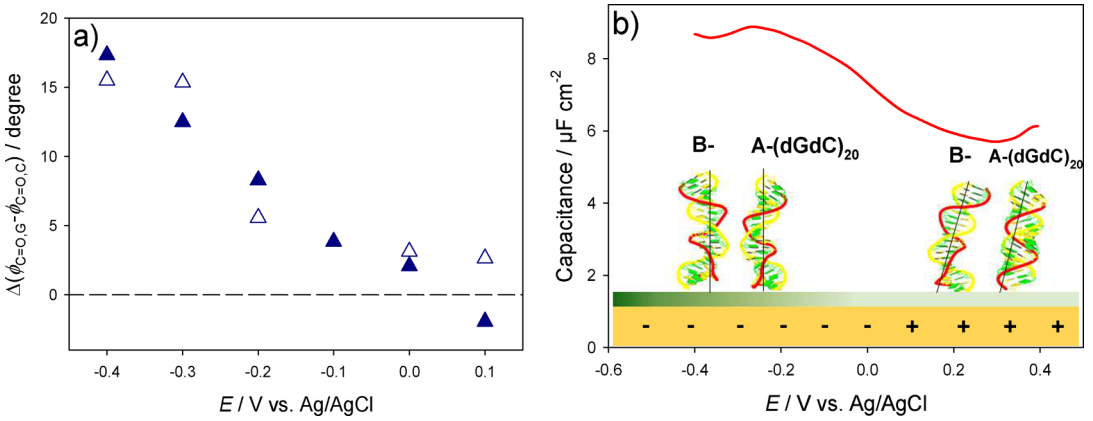

Figure 11. (a) Potential dependence of the difference between ($\phi_{C=O,G} - \phi_{C=O,C}$) calculated from the data of the tilt angles of the carbonyl stretching modes in $(dGdC)_{20}$ monolayers on the Au surface. The filled symbols are negative and the open symbols are positive potential scans, respectively. (b) Representative capacitance−potential dependence of the $(dGdC)_{20}$-modified Au electrode and a schematic illustration of the orientation of the $(dGdC)_{20}$ duplexes on Au at E = 0.3 and E = −0.4 V. dC is marked with yellow and dG with green. The DNA structures were calculated based on the results obtained in this work using the 3dna software package.[70]

facilitates understanding of the DNA hybridization−dehybridization process in monolayers adsorbed on solid surfaces and possible electric field implications in the electron transport phenomenon via the DNA double helix that might be compromised by applying the structure-disturbing potential to the conductive substrates. This information is crucial for the development of DNA sensors and chips, DNA-templated bioelectronics circuits, and bioelectronic devices exploiting the inherent DNA duplex conductivity.[71]

■ ASSOCIATED CONTENT

Supporting Information

The Supporting Information is available free of charge on the ACS Publications website at DOI: 10.1021/acs.jpcb.6b12363.

In situ PM IRRA spectra originating from the 6-marcapto1-hexanol molecules in the dsDNA/6-mercapro1-hexanol monolayer, isotropic optical constants of $(dAdT)_{25}$ and $(dGdC)_{20}$ duplexes, description of the approach used to calculate the spectra of randomly distributed molecules in a monolayer thick film, and examples of band deconvolution of the 1800−1500 cm^{-1} PM IRRA spectra of dsDNA monolayers adsorbed on the Au surface[64] (PDF)

■ AUTHOR INFORMATION

Corresponding Authors

*E-mail: elena.ferapontova@inano.au.dk; Phone: +45-87156703; Fax: +45-87154041.

*E-mail: izabella.brand@uni-oldenburg.de; Phone: +49-441-798-3973; Fax: +49-441-798-3979.

ORCID

Elena E. Ferapontova: 0000-0003-1177-3204

Izabella Brand: 0000-0002-7710-0021

Notes

The authors declare no competing financial interest.

■ ACKNOWLEDGMENTS

The work was supported by the Danish National Research Foundation (DNRF) through their support to the CDNA, grant number DNRF81. We thank Mr. Michael Rosholm

DOI: 10.1021/acs.jpcb.6b12363
J. Phys. Chem. B XXXX, XXX, XXX−XXX

Mortensen for his kind assistance in DNA labelling with methylene blue.

REFERENCES

(1) Fritzsche, W. *DNA-Based Molecular Electronics: International Symposium on DNA-Based Molecular Electronics*. AIP Conference Proceedings: Jena, Germany, 13−15 May 2004; Vol. *725*.

(2) Sassolas, A.; Leca-Bouvier, B. D.; Blum, L. J. DNA biosensors and microarrays. *Chem. Rev. (Washington, DC, U. S.)* **2008**, *108*, 109−139.

(3) Kjems, J.; Ferapontova, E. E.; Gothelf, K. V. *Nucleic Acid Nanotechnology*; Springer: Heidelberg, 2014.

(4) Boussicault, F.; Robert, M. Electron transfer in DNA and in DNA-related biological processes. Electrochemical insights. *Chem. Rev. (Washington, DC, U. S.)* **2008**, *108*, 2622−2645.

(5) Zaffino, R. L.; Galan, T.; Pardo, W. A.; Mir, M.; Samitier, J. Nanoprobes for enhanced electrochemical DNA sensors. *Wiley Interdiscip. Rev. Nanomed. Nanobiotechnol.* **2015**, *7*, 817−827.

(6) Palecek, E.; Bartosik, M. Electrochemistry of nucleic acids. *Chem. Rev. (Washington, DC, U. S.)* **2012**, *112*, 3427−3481.

(7) Furst, A. L.; Hill, M. G.; Barton, J. K. Electrocatalysis in DNA sensors. *Polyhedron* **2014**, *84*, 150−159.

(8) Muren, N. B.; Olmon, E. D.; Barton, J. K. Solution, surface, and single molecule platforms for the study of DNA-mediated charge transport. *Phys. Chem. Chem. Phys.* **2012**, *14*, 13754−13771.

(9) Janegitz, B. C.; Cancino, J.; Zucolotto, V. Disposable biosensors for clinical diagnosis. *J. Nanosci. Nanotechnol.* **2014**, *14*, 378−389.

(10) Walcarius, A.; Minteer, S. D.; Wang, J.; Lin, Y.; Merkoci, A. Nanomaterials for bio-functionalized electrodes: recent trends. *J. Mater. Chem. B* **2013**, *1*, 4878−4908.

(11) Braun, E.; Eichen, Y.; Sivan, U.; Ben-Yoseph, G. DNA-templated assembly and electrode attachment of a conducting silver wire. *Nature (London, U. K.)* **1998**, *391*, 775−778.

(12) Keren, K.; Berman, R. S.; Buchstab, E.; Sivan, U.; Braun, E. DNA-templated carbon nanotube field-effect transistor. *Science (Washington, DC, U. S.)* **2003**, *302*, 1380−1382.

(13) Campos, R.; Zhang, S.; Majikes, J. M.; Ferraz, L. C. C.; LaBean, T. H.; Dong, M. D.; Ferapontova, E. E. Electronically addressable nanomechanical switching of i-motif DNA origami assembled on basal plane HOPG. *Chem. Commun. (Cambridge, U. K.)* **2015**, *51*, 14111−14114.

(14) Bell, N. A. W.; Keyser, U. F. Digitally encoded DNA nanostructures for multiplexed, single-molecule protein sensing with nanopores. *Nat. Nanotechnol.* **2016**, *11*, 645−651.

(15) Papadopoulou, E.; Gale, N.; Thompson, J. F.; Fleming, T. A.; Brown, T.; Bartlett, P. N. Specifically horizontally tethered DNA probes on Au surfaces allow labelled and label-free DNA detection using SERS and electrochemically driven melting. *Chem. Sci.* **2016**, *7*, 386−393.

(16) Steel, A. B.; Herne, T. M.; Tarlov, M. J. Electrochemical quantitation of DNA immobilized on gold. *Anal. Chem. (Washington, DC, U. S.)* **1998**, *70*, 4670−4677.

(17) Hansen, M. N.; Farjami, E.; Kristiansen, M.; Clima, L.; Pedersen, S. U.; Daasbjerg, K.; Ferapontova, E. E.; Gothelf, K. V. Synthesis and application of a triazene-ferrocene modifier for immobilization and characterization of oligonucleotides at electrodes. *J. Org. Chem.* **2010**, *75*, 2474−2481.

(18) Johnson, R. P.; Gale, N.; Richardson, J. A.; Brown, T.; Bartlett, P. N. Denaturation of dsDNA immobilised at a negatively charged gold electrode is not caused by electrostatic repulsion. *Chem. Sci.* **2013**, *4*, 1625.

(19) Johnson, R. P.; Richardson, J. A.; Brown, T.; Bartlett, P. N. Real-time surface-enhanced Raman spectroscopy monitoring of surface pH during electrochemical melting of double-stranded DNA. *Langmuir* **2012**, *28*, 5464−5470.

(20) Papadopoulou, E.; Goodchild, S. A.; Cleary, D. W.; Weller, S. A.; Gale, N.; Stubberfield, M. R.; Brown, T.; Bartlett, P. N. Using surface-enhanced Raman spectroscopy and electrochemically driven melting to discriminate *Yersinia pestis* from *Y. pseudotuberculosis* based on single nucleotide polymorphisms within unpurified polymerase chain reaction amplicons. *Anal. Chem. (Washington, DC, U. S.)* **2015**, *87*, 1605−1612.

(21) Kumar, K. S.; Naaman, R. Quantitative analysis and characterization of self-assembled DNA on a silver surface. *Langmuir* **2012**, *28*, 14514−14517.

(22) Xie, Z.; Markus, T. Z.; Cohen, S. R.; Vager, Z.; Gutierrez, R.; Naaman, R. Spin specific electron conduction through DNA oligomers. *Nano Lett.* **2011**, *11*, 4652−4655.

(23) Kelley, S. O.; Barton, J. K.; Jackson, N. M.; McPherson, L. D.; Potter, A. B.; Spain, E. M.; Allen, M. J.; Hill, M. G. Orienting DNA helices on gold using applied electric fields. *Langmuir* **1998**, *14*, 6781−6784.

(24) Mahajan, S.; Richardson, J.; Brown, T.; Bartlett, P. N. SERS-melting: A new method for discriminating mutations in DNA sequences. *J. Am. Chem. Soc.* **2008**, *130*, 15589−15601.

(25) Farjami, E.; Campos, R.; Ferapontova, E. E. Effect of the DNA end of tethering to electrodes on electron transfer in methylene blue-labeled DNA duplexes. *Langmuir* **2012**, *28*, 16218−16226.

(26) Josephs, E. A.; Ye, T. Electric-field dependent conformations of single DNA molecules on a model biosensor surface. *Nano Lett.* **2012**, *12*, 5255−5261.

(27) Rant, U.; Arinaga, K.; Fujita, S.; Yokoyama, N.; Abstreiter, G.; Tornow, M. Electrical manipulation of ologonucleotides grafted to charged surfaces. *Org. Biomol. Chem.* **2006**, *4*, 3448−3455.

(28) Rant, U.; Arinaga, K.; Fujita, S.; Yokoyama, N.; Abstreiter, G.; Tornow, M. Dynamic electrical switching of DNA layers on a metal surface. *Nano Lett.* **2004**, *4*, 2441−2445.

(29) Gebala, M.; Bonilla, S.; Bisaria, N.; Herschlag, D. Does cation size affect occupancy and electrostatic screening of the nucleic acid ion atmosphere? *J. Am. Chem. Soc.* **2016**, *138*, 10925−10934.

(30) Giambasu, G. M.; Gebala, M. K.; Panteva, M. T.; Luchko, T.; Case, D. A.; York, D. M. Competitive interaction of monovalent cations with DNA from 3D-RISM. *Nucleic Acids Res.* **2015**, *43*, 8405−8415.

(31) Mohilner, D. M. The electrical double layer, Part 1: Elements of double layer theory. In *Electroanal. Chem.*; Bard, A. J., Ed.; Marcel Dekker, Inc.: New York, 1966; Vol. *1*, pp 241−405.

(32) Palecek, E. Normal pulse polarography of double-helical DNA: Dependence of the wave height on starting potential. *Collect. Czech. Chem. Commun.* **1974**, *39*, 3449−3455.

(33) Valenta, P.; Nürnberg, H. W. The electrochemical behaviour of DNA at electrically charged interfaces. *Biophys. Struct. Mech.* **1974**, *1*, 17−26.

(34) Heaton, R. J.; Peterson, A. W.; Georgiadis, R. M. Electrostatic surface plasmon resonance: Direct electric field-induced hybridization and denaturation in monolayer nucleic acid films and label-free discrimination of base mismatches. *Proc. Natl. Acad. Sci. U. S. A.* **2001**, *98*, 3701−3704.

(35) Tatulian, S. A. Structural characterization of membrane proteins and peptides by FTIR and ATR-FTIR spectroscopy. In *Lipid-protein interactions. Methods and protocols*; Kleinschmidt, J. H., Ed.; Springer: New York, 2013; pp 177−218.

(36) Brand, I. Application of polarization modulation infrared reflection absorption spectroscopy under electrochemical control for structural studies of biomimetic assemblies. *Z. Phys. Chem.* **2016**, *230*, 133−183.

(37) Mirabella, F. M. *Modern techniques in applied molecular spectroscopy*; John Wiley and Sons, Inc.: New York, 1998.

(38) Golden, W. G.; Dunn, D. S.; Overend, J. A method for measuring infrared reflection-absorption spectra of molecules adsorbed on low-area surfaces at monolayer and submonolayer concentrations. *J. Catal.* **1981**, *71*, 395−404.

(39) Kycia, A. H.; Su, Z. F.; Brosseau, C. L.; Lipkowski, J. In situ PM-IRRAS studies of biomimetic membranes supported at a gold electrode surface. In *Vibration spectroscopy at electrified interfaces*; Wieckowski, A., Korzeniewski, C., Braunschweig, B., Eds.; Willey: Heidelberg, 2013; pp 345−417.

DOI: 10.1021/acs.jpcb.6b12363
J. Phys. Chem. B XXXX, XXX, XXX−XXX

(40) Lee, C.; Cho, M. Vibrational dynamics of DNA. II: Deuterium exchange effects and simulated IR absorption spectra. *J. Chem. Phys.* **2006**, *125*, 114509.
(41) Lee, C.; Park, K. H.; Cho, M. Vibrational dynamics of DNA. I. Vibrational basis modes and couplings. *J. Chem. Phys.* **2006**, *125*, 114508.
(42) Markham, R. M.; Zuker, M. DINAMelt web server for nucleic acid melting prediction. *Nucleic Acids Res.* **2005**, *33*, W577−W581.
(43) Abi, A.; Ferapontova, E. E. Unmediated by DNA electron transfer in redox-labeled DNA duplexes end-tethered to gold electrodes. *J. Am. Chem. Soc.* **2012**, *134*, 14499−14507.
(44) Abi, A.; Lin, M.; Pei, H.; Fan, C.; Ferapontova, E. E.; Zuo, X. Electrochemical switching with 3D DNA tetrahedral nanostructures self-assembled at gold electrodes. *ACS Appl. Mater. Interfaces* **2014**, *6*, 8928−8931.
(45) Rosen, C. B.; Kodal, A. L. B.; Nielsen, J. S.; Schaffert, D. H.; Scavenius, C.; Okholm, A. H.; Voigt, N. V.; Enghild, J. J.; Kjems, J.; Tørring, T.; Gothelf, K. V. Template-directed covalent conjugation of DNA to native antibodies, transferrin and other metal-binding proteins. *Nat. Chem.* **2014**, *6*, 804−809.
(46) Zawisza, I.; Bin, X.; Lipkowski, J. Spectroelectrochemical studies of bilayers of phospholipids in gel and liquid state on Au(111) electrode surface. *Bioelectrochemistry* **2004**, *63*, 137−147.
(47) Kuznetsov, V.; Papastavrou, G. Ion adsorption on modified electrodes as determined by direct force measurements under potentiostatic control. *J. Phys. Chem. C* **2014**, *118*, 2673−2685.
(48) Walczak, M. W.; Popenoe, D. D.; Deinhammer, R. S.; Lamp, B. D.; Chung, C.; Porter, M. D. Reductive desorption of alkanethiolate monolayers at gold: A measure of surface coverage. *Langmuir* **1991**, *7*, 2687−2693.
(49) Widrig, C. A.; Chung, C.; Porter, M. D. The electrochemical desorption of n-alkanethiol monolayers from polycrystalline Au and Ag electrodes. *J. Electroanal. Chem. Interfacial Electrochem.* **1991**, *310*, 335−359.
(50) Arinaga, K.; Rant, U.; Knežević, J.; Pringsheim, E.; Tornow, M.; Fujita, S.; Abstreiter, G.; Yokoyama, N. Controlling the surface density of DNA on gold by electrically induced desorption. *Biosens. Bioelectron.* **2007**, *23*, 326−331.
(51) Hartwich, G.; Caruana, D. J.; de Lumley-Woodyear, T.; Wu, Y.; Campbell, C. N.; Heller, A. Electrochemical study of electron transport through thin DNA films. *J. Am. Chem. Soc.* **1999**, *121*, 10803−10812.
(52) Peterlinz, K. A.; Georgiadis, R. M.; Herne, T. M.; Tarlov, M. J. Observation of hybridization and dehybridization of thiol-tethered DNA using two-color surface plasmon resonance spectroscopy. *J. Am. Chem. Soc.* **1997**, *119*, 3401−3402.
(53) Anderson, M. R.; Gatin, M. Effect of applied potential upon the *in situ* structure of self -assembled monolayers on gold electrodes. *Langmuir* **1994**, *10*, 1638−1641.
(54) Tsuboi, M. Application of infrared spectroscopy to structure studies of nucleic acids. *Appl. Spectrosc. Rev.* **1970**, *3*, 45−90.
(55) Lee, C.; Cho, M. Vibrational dynamics of DNA: IV. Vibrational spectroscopic characteristics of A-, B-, and Z-from DNA's. *J. Chem. Phys.* **2007**, *126*, 14102.
(56) Taniguchi, H.; Saito, M. The effect of water in water on infrared spectra of DNA. *J. Phys. Condens. Matter* **2009**, *21*, 064242.
(57) Moskovits, M. Surface selection rules. *J. Chem. Phys.* **1982**, *77*, 4408−4416.
(58) Allara, D. L.; Nuzzo, R. G. Spontaneously organized molecular assemblies. 2. Quantitative infrared spectroscopic determination of equilibrium structures of solution - adsorbed n-alkanoic acids on an oxidized aluminum surface. *Langmuir* **1985**, *1*, 52−66.
(59) Allara, D. L.; Swalen, J. D. An infrared reflection spectroscopy study of oriented cadmium arachidate monolayer films on evaporated silver. *J. Phys. Chem.* **1982**, *86*, 2700−2704.
(60) Levicky, R.; Herne, T. M.; Tarlov, M. J.; Satija, S. K. Using self-assembly to control the structure of DNA monolayers on gold: a neutron reflectivity study. *J. Am. Chem. Soc.* **1998**, *120*, 9787−9792.
(61) Sam, M.; Boon, E. M.; Barton, J. K.; Hill, M. G.; Spain, E. M. Morphology of 15-mer duplexes tethered to Au(111) probed using scanning probe microscopy. *Langmuir* **2001**, *17*, 5727−5730.
(62) Josephs, E. A.; Ye, T. A single-molecule view of conformational switching of DNA tethered to a gold electrode. *J. Am. Chem. Soc.* **2012**, *134*, 10021−10030.
(63) Shimanouchi, T.; Tsuboi, M.; Kyogoko, Y. *Infrared spectra of nucleic acids and related compounds*; Interscience: New York, 1964; Vol. 7, pp 467−499.
(64) Wood, B. R. The importance of hydration and DNA conformation in interpreting infrared spectra of cells and tissues. *Chem. Soc. Rev.* **2016**, *45*, 1999−2018.
(65) Pilet, J.; Brahms, J. Investigation of DNA structural changes by infrared spectroscopy. *Biopolymers* **1973**, *12*, 387−403.
(66) Lu, K. C.; Prohofsky, E. W.; van Zandt, L. L. Vibrational modes of A-DNA, B-DNA, and A-RNA backbones: an application of a green-function refinement procedure. *Biopolymers* **1977**, *16*, 2491−2506.
(67) Pilet, J.; Brahms, J. Dependence of B-A conformation change in DNA on base composition. *Nature New Biology* **1972**, *236*, 99−100.
(68) Harris, W. E. Interactions between fluorescent labeled phosphatidyl serine and cations. *Chem. Phys. Lipids* **1977**, *19*, 243−254.
(69) Cruse, W. B. T.; Salisbury, S. A.; Brown, T.; Cosstick, R.; Eckstein, F.; Kennard, O. Chiral phosphorothioate analogues of B-DNA the crystal structure of Rp-dlGp(S)CpGp(S)CpGp(S)Cl. *J. Mol. Biol.* **1986**, *192*, 891−905.
(70) Lu, X. J.; Olson, W. K. 3DNA: a software package for the analysis, rebuilding and visualization of three-dimensional nucleic acid structures. *Nucleic Acids Res.* **2003**, *31*, 5108−5121.
(71) Ferapontova, E. E. Hybridization biosensors relying on electrical properties of nucleic acids. *Electroanalysis* **2017**, *29*, 6−13.

DOI: 10.1021/acs.jpcb.6b12363
J. Phys. Chem. B XXXX, XXX, XXX−XXX